

Degradation-Aware Microgrid Optimal Planning: Integrating Dynamic Energy Efficiencies and Second-Life Battery Potential

Hassan Zahid Butt and Xingpeng Li, *Senior Member, IEEE*

Abstract— Traditional microgrid planning often overlooks PV and BESS degradation or relies on complex, downscaled models, leading to unreliable, costly and suboptimal investment decisions. This paper presents a degradation-based investment optimization (DBIO) methodology for long-term microgrid planning. The model optimally sizes and schedules PV, BESS, and controllable distributed energy resources, while considering technical, financial, and degradation characteristics. We first developed a cumulative multi-year optimization model as a benchmark, excluding BESS efficiency fade and capacity degradation that would be captured in the next step, to ensure convergence. Subsequently, a yearly validation model was iteratively solved for each year in the planning horizon, updating energy efficiencies of PV and BESS, along with BESS capacity, based on annual degradation, ensuring the reliability of initial solution. An iterative refinement process further adjusts BESS capacity to eliminate load shedding while minimizing costs. Sensitivity analyses on PV efficiency degradation rates, second-life battery (SLB) capital cost, and grid tariffs further explore their economic implications. Results show that degradation significantly impacts resource allocation, with ignored degradation risking reliability, potential load shedding, and blackout costs, while SLBs provide cost-saving opportunities. The DBIO framework offers a computationally efficient and scalable solution for microgrid planning, with broader applications in grid-scale asset management.

Index Terms— Battery energy storage systems, capacity fade, efficiency fade, iterative optimization, microgrid planning, mixed-integer linear programming, PV degradation, renewable energy integration, second-life batteries

NOMENCLATURE

Sets:

Y Set of total number of years
 D Set of representative days in a single year
 T Set of hourly time periods in a single day

Indices:

y Year y , an element of set Y
 d Day d , an element of set D
 t Time period t , an element of set T

Parameters:

$p_{y,d,t}^{load}$ Total load (MW) in year y , day d , & hour t
 $p_{y,d,t}^{PV}$ Solar power capacity factor in year y , day d , & hour t
 C_{CDER}^{op} C-DER operational cost factor (\$/MW)
 C_{CDER}^{nl} C-DER no-load cost (\$/h)
 $C_{CDER}^{capital}$ C-DER capital cost factor (\$/MW)
 $C_{PV}^{capital}$ PV capital cost factor (\$/MW)
 $C_{BESS}^{capital}$ BESS capital cost factor (\$/MWh)
 δ_{BESS}^{deg} BESS degradation cost factor (\$/MWh)
 C_{grid}^{imp} Grid import power cost factor (\$/MW)

C_{grid}^{exp} Grid export power cost factor (\$/MW)
 γ_{PV}^{rep} PV replacement cost as a percent of capital cost
 γ_{BESS}^{rep} BESS replacement cost as a percent of capital cost
 T_{BESS}^{chg} Duration of BESS charging (h)
 T_{BESS}^{dchg} Duration of BESS discharging (h)
 P_{BESS}^{min} C-DER minimum output power (MW)
 η_{BESS} BESS roundtrip cycle efficiency
 η_{PV}^{init} Initial PV conversion efficiency
 SOC_{max} Maximum state of charge limit for BESS
 SOC_{min} Minimum state of charge limit for BESS
 DOD BESS depth of discharge
 CL_{dod}^{max} BESS cycle life at maximum DOD
 CL_{dod} BESS cycle life at any DOD
 δ_{PV}^{deg} PV efficiency degradation rate per annum
 $C_{LS}^{penalty}$ Penalty cost factor for load shedding (\$/MW)
 $BigM$ A very large number
 Y_{MG} Total microgrid planning years
 SOH_{init} Initial BESS state of health
 SOH_y BESS state of health at year y
 P_{tie}^{max} Max import or export power (MW) from/to grid
 α Scaling factor for repeating load and solar profiles

Variables:

P_{CDER}^{max} C-DER maximum output power (MW)
 $P_{y,d,t}^{imp}$ Grid import power (MW) in year y , day d , & hour t
 $P_{y,d,t}^{exp}$ Grid export power (MW) in year y , day d , & hour t
 S_{PV} PV system size (MW)
 S_{BESS} BESS energy capacity (MWh)
 $P_{y,d,t}^{CDER}$ C-DER output power (MW) in year y , day d , & hour t
 $P_{y,d,t}^{PV}^{curt}$ PV power curtailed (MW) in year y , day d , & hour t
 $PLS_{y,d,t}$ Load shed (MW) in year y , day d , & hour t
 $P_{y,d,t}^{chg}$ BESS charge power (MW) in year y , day d , & hour t
 $P_{y,d,t}^{dchg}$ BESS discharge power (MW) in year y , day d , & hour t
 E_{BESS}^{init} Initial BESS energy level (MWh)
 $E_{y,d,t}^{BESS}$ Energy level of BESS (MWh) in year y , day d , & hour t
 C_{PV}^{deg} PV degradation cost (\$)
 C_{BESS}^{deg} BESS degradation cost (\$)
 $U_{y,d,t}^{chg}$ BESS charging status in year y , day d , & hour t
 $U_{y,d,t}^{dchg}$ BESS discharging status in year y , day d , & hour t
 $U_{y,d,t}^{CDER}$ C-DER commitment status in year y , day d , & hour t
 $U_{y,d,t}^{imp}$ Grid import status in year y , day d , & hour t
 $U_{y,d,t}^{exp}$ Grid export status in year y , day d , & hour t
 η_y^{PV} PV conversion efficiency in year y
 MS Model selector – Binary variable to toggle capital cost in the objective function.

I. INTRODUCTION

Microgrids (MGs) have become integral to modern power systems, enabling the transition toward decentralized, resilient energy networks essential for achieving global sustainability goals [1]. By facilitating localized energy

Hassan Zahid Butt and Xingpeng Li are with the Department of Electrical and Computer Engineering, University of Houston, Houston, TX, 77204, USA. (e-mail: hbutt@uh.edu; xli82@uh.edu).

generation and storage, MGs reduce dependence on centralized grids, mitigate transmission losses, and improve energy access in remote or underserved regions [2].

The integration of renewable energy sources (RES), particularly solar photovoltaic (PV) systems, has been instrumental in driving MG adoption due to their low operational costs, scalability, and environmental benefits [3], [4]. However, the intermittent nature of solar energy requires complementary energy storage solutions to ensure a stable energy supply, particularly in remote MGs without grid support [5]. Among available storage technologies, battery energy storage systems (BESS) have become prominent due to their high energy density, scalability (from residential to utility-scale applications), and minimal geographic constraints, compared to alternatives such as pumped hydro storage [6]–[8]. The combination of PV and BESS enables continuous power delivery within MGs, even during low solar output periods, enhancing energy autonomy, reducing reliance on fossil fuels, and advancing sustainability objectives, while also improving overall system resilience [9].

Despite these advantages, high capital costs of PV and BESS remain a significant barrier to widespread MG adoption. Proper sizing of these systems is critical for economic viability, as over- or under-sizing can compromise financial feasibility and/or operational reliability [10]. Moreover, PV and BESS components inevitably degrade over time, introducing further complexities to MG planning [11], [12]. The degradation dynamics of PV systems and BESS are distinct yet critical. PV panels typically experience a gradual reduction in output efficiency mainly impacted by environmental conditions factors—such as ultraviolet radiation exposure, thermal cycling, and humidity—and follows a constant annual degradation rate. Additionally, PV degradation costs are typically a fraction of the initial investment, proportional to the system size, while BESS systems experience both energy capacity and roundtrip efficiency degradation due to operation and aging effects [13]. Figure 1 presents the average solar efficiency degradation rate per year provided by a report from the National Renewable Energy Laboratory (NREL) [14].

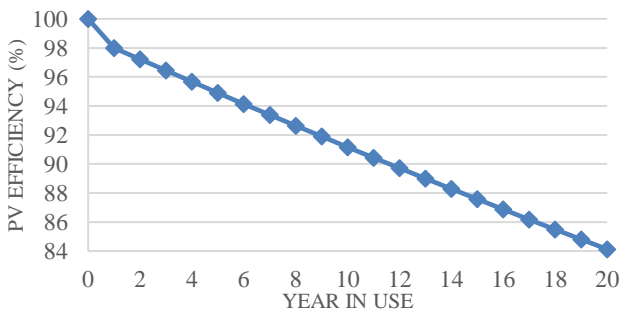


Figure 1. Average PV efficiency degradation per annum.

In MGs, technology degradation has direct implications for power reliability and lifecycle costs, as a degraded resource may require earlier replacement or necessitate larger initial capacity to maintain desired performance. Failure to incorporate these degradation profiles into MG planning models can lead to suboptimal designs, increased operational challenges, and higher long-term costs, highlighting the importance of a flexible and degradation-aware approach.

Concurrently, the global battery market—valued at \$112 billion in 2021 and projected to grow to \$424 billion by 2030—has seen lithium-ion technology dominate due to advancements in energy density and cost reductions [15], [16]. The rapid adoption of electric vehicles (EVs) has contributed to this growth, with an estimated 250,000 tons of EV batteries reaching end-of-life annually in Europe by 2030 [17]. These end-of-life batteries present three primary management options: disposal, recycling, or repurposing into second-life batteries (SLBs) for less demanding applications [18].

Disposal is the least favorable due to environmental risks, as evidenced by incidents such as landfill fires caused by discarded batteries [19]. Recycling, while essential for sustaining the mineral supply chain, remains economically challenging without subsidies, due to its reliance on technical expertise, local manufacturing capacity, and supportive policies [20], [21]. In contrast, repurposing EV batteries as SLBs offers a cost-effective, sustainable pathway for stationary applications, such as MGs, where reliability is critical, and budgets are constrained [22]. Figure 2 shows the current end-of-life battery management strategy under study.

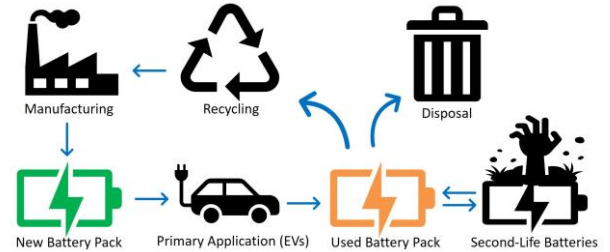


Figure 2. EV BESS end-of-life management strategy.

The expected growth in EV adoption creates a substantial opportunity for SLBs to reduce storage costs and enable greater integration of renewable energy into MGs and broader grid systems. This paper aims to address these challenges by exploring degradation-aware MG planning while assessing the economic potential of SLBs in long-term MG optimization. The following section reviews the existing literature on MG planning approaches, degradation modeling, and SLB applications, identifying key gaps that motivate the need for a comprehensive long-term planning framework.

II. LITERATURE REVIEW

The optimal planning and operation of PV-BESS microgrids have been widely studied, with early models primarily focusing on cost optimization and net present value [23], [24]. Many of these deterministic models, such as those in [25], [26], simplify degradation effects by assuming constant rates (e.g., 1% or 5% annually), omitting complex degradation dynamics critical for long-term accuracy. Recent advancements have introduced multi-objective optimization frameworks that balance economic and technical constraints. Meta-heuristic techniques, such as genetic algorithms and particle swarm optimization, have been applied to optimize PV-BESS sizing while improving system stability [27], [28]. However, many of these studies overlook degradation, limiting accuracy in lifetime cost estimation.

To address uncertainties in renewable generation and load variability, stochastic optimization approaches have been developed for MG planning, particularly for applications like

peak shaving and voltage regulation [29], [30]. However, many of these models assume linear capacity degradation, which, while computationally efficient, fails to capture real-world battery aging effects, reducing the accuracy of long-term economic assessments.

Empirical and semi-empirical degradation models have provided insights into the influence of state-of-charge (SOC) and depth-of-discharge (DOD) on battery cycle life [31]. However, these models introduce non-linear dependencies that increase computation times and complicate convergence. Similarly, machine learning-based approaches have been proposed to predict BESS degradation [32], but their reliance on low temporal resolution often compromises model reliability. The use of BESS for behind-the-meter and stackable applications has also been studied, particularly in optimal sizing for peak load shaving, voltage stabilization, and reliability enhancement [33]. However, these studies frequently overlook replacement costs due to capacity degradation, making their economic conclusions less robust.

Accelerated degradation testing has been introduced to estimate BESS capacity loss under various stress conditions [34]. Although promising for precise degradation prediction, these models are computationally intensive, potentially limiting their suitability for all MG applications. Further studies, such as [35]-[37], model dynamic capacity changes in BESS, but they often neglect efficiency degradation in PV and BESS systems and fail to incorporate second-life potential in long-term MG planning.

Several studies demonstrated that battery energy efficiency declines over time, yet this remains largely unaccounted for, particularly in SLBs. While capacity fade is well-documented, the degradation of round-trip energy efficiency (RTE) is often assumed minimal or remains unquantified. As discussed in [38], RTE declines to approximately 80% when batteries reach 80% state-of-health (SOH). Similarly, research in [39] indicates that for lithium iron phosphate (LFP) batteries, RTE degrades from 95% to 91% over their operational lifespan. Comparative analyses presented in [40] reveal that energy arbitrage accelerates capacity degradation nearly twice as fast as frequency regulation, with NMC+LMO batteries exhibiting a 1% RTE reduction over 1,200 cycles, whereas LFP chemistry remains more stable under similar conditions. Additionally, real-world studies on electric bus batteries, as reported in [41], demonstrate an RTE decline ranging from 0.46% to 0.86% over a 3.5-year period, reinforcing the necessity of incorporating efficiency degradation in microgrid planning. However, the above-mentioned studies do not integrate efficiency fade into long-term MG optimization frameworks, leaving a critical gap in accurately modeling SLB performance. Overlooking these risks system reliability, energy availability, and overall economic feasibility in long-term MG investment and operational planning.

A. Research Gaps

Despite advancements in microgrid planning, key gaps persist, particularly in capturing long-term degradation effects and balancing computational efficiency with modeling accuracy. These gaps can be summarized as follows:

- i. Overly complex optimization methods require downscaled temporal resolutions for computational feasibility. These simplifications can overlook critical

temporal variations, potentially compromising long-term reliability and accuracy.

- ii. While BESS capacity fade is widely considered, PV and BESS efficiency degradation is often omitted. Such gradual efficiency reduction can significantly impact energy production, operational reliability, and financial assessments, particularly in long-term planning.
- iii. Existing SLB models focus primarily on cost savings, failing to account for the compounded effects of capacity and efficiency degradation. This leads to overestimated financial viability and underestimated performance risks in MG applications.

B. Contributions

This study develops a degradation-based investment optimization (DBIO) framework to enhance MG planning by integrating a multi-year optimization model, a yearly validation process for PV and BESS degradation, and an iterative refinement mechanism for system sizing. DBIO ensures degradation-aware investment decisions while maintaining cost-effectiveness and reliability. The key contributions of this study are as follows:

- i. Develops a degradation-aware MG planning framework that integrates PV efficiency fading, and BESS capacity and energy efficiency degradation into a long-term investment and operational strategy, improving accuracy in MG cost and performance.
- ii. Evaluates SLBs' combined effects of reduced capacity, efficiency decline, and lower capital cost, providing a practical economic analysis that reflects real-world performance constraints.
- iii. Introduces a high-resolution iterative approach that maintains computational efficiency while refining MG investment decisions, minimizing load shedding risk, and enhancing system reliability.
- iv. Conducts comparative analysis between binary search-based model refinement and fixed-step incremental approaches, along with sensitivity studies on PV degradation rates, SLB cost reduction, and grid tariff variations, demonstrating model robustness under diverse technical and economic conditions.

III. PROPOSED METHODOLOGY

In a DBIO framework for MG planning problem, the objective is to minimize total costs, comprising: (1) one-time capital investment costs, (2) maintenance and operational costs, and (3) degradation or replacement costs, where applicable. This study begins by developing a cumulative optimization model referred to as the "integrated multi-year model" for MG planning, serving as a benchmark. The benchmark model optimizes the sizes of controllable distributed energy resource (C-DER), PV system, and BESS, while developing an operational strategy over the planning period. The model is designed to accommodate a full year of hourly load and solar capacity factor data, along with grid tariff information, ensuring high-resolution decision-making. To extend these data over the planning horizon, DBIO generates yearly profiles by replicating the base year data while incorporating a realistic annual load growth rate. Although this study utilizes a high-resolution approach, the model is structured to also support downscaled temporal

resolutions, such as using representative days or months to approximate yearly variations. This adaptability provides a balance between computational efficiency and solution accuracy, making it applicable to more complex larger-scale MG planning scenarios where necessarily reducing problem size.

Building on this framework, the DBIO methodology also accounts for PV efficiency degradation, which follows a predictable annual decline independent of operational usage. In contrast, BESS capacity and efficiency degradation are usage-dependent, making them more complex to model within the initial optimization. To maintain computational efficiency and avoid potential convergence issues, these degradation effects are excluded from the benchmark model. However, since BESS degradation can significantly impact system performance over time, the investment decisions derived from the integrated multi-year model require further validation. To address this, DBIO introduces a "yearly validation model", employing a post-optimization data analysis approach. This model systematically updates PV efficiency, BESS efficiency, and BESS capacity on an annual basis according to their respective degradation profiles, ensuring a more accurate representation of system reliability and long-term performance.

Furthermore, an iterative optimization process within DBIO refines BESS sizing, ensuring zero load shedding while achieving 100% reliability at minimal cost. Given the iterative nature of the approach, maintaining computational efficiency is crucial, particularly in large-scale or high-resolution simulations where excessive iterations can lead to prohibitive computational expense. A comparison of two refinement methods—Fixed Step Increments and Binary Search Algorithm—illustrates the trade-off between solution precision and convergence speed. The binary search approach, in particular, significantly reduces iterations compared to fixed step adjustments, making it a computationally efficient method within DBIO for optimizing investment decisions.

A. Integrated Multi-year Model

The objective function for this model, presented in (1), includes the operational and no-load costs of the C-DER, along with capital costs for C-DER, PV, and BESS, as well as degradation costs associated with PV and BESS. While capital costs are incurred only once, operational and degradation costs are computed annually over the planning horizon. To penalize load shedding, a high penalty cost is associated with unserved load and incorporated into the objective function. The model also accounts for the financial impact of grid interactions, incorporating both the cost of imported electricity and the revenue from exported surplus energy to ensure an optimal energy exchange strategy.

$$\begin{aligned} \min \alpha \cdot \sum_{y \in Y} \sum_{d \in D} \sum_{t \in T} & (P_{y,d,t}^{CDER} \cdot C_{CDER}^{op} + U_{y,d,t}^{CDER} \cdot C_{CDER}^{nl}) \\ & + MS \cdot (P_{CDER}^{max} \cdot C_{CDER}^{capital} + S_{PV} \cdot C_{PV}^{capital} + \\ & S_{BESS} \cdot C_{BESS}^{capital}) + C_{PV}^{deg} \cdot Y_{MG} + \alpha \cdot C_{BESS}^{deg} \\ & + \alpha \cdot \sum_{y \in Y} \sum_{d \in D} \sum_{t \in T} (P_{y,d,t}^{LS} \cdot C_{LS}^{penalty}) + \\ & \alpha \cdot \sum_{y \in Y} \sum_{d \in D} \sum_{t \in T} (P_{y,d,t}^{imp} \cdot C_{grid}^{imp}) - \\ & \alpha \cdot \sum_{y \in Y} \sum_{d \in D} \sum_{t \in T} (P_{y,d,t}^{exp} \cdot C_{grid}^{exp}) \end{aligned} \quad (1)$$

The constraints governing this model are as follows:

$$P_{y,d,t}^{CDER} + P_{y,d,t}^{dchg} + (\eta_y^{PV} \cdot P_{y,d,t}^{PV} \cdot S_{PV}) + P_{y,d,t}^{LS} + P_{y,d,t}^{imp} \quad (2)$$

$$= P_{y,d,t}^{load} + P_{y,d,t}^{chg} + P_{y,d,t}^{pvcurt} + P_{y,d,t}^{exp} \quad (3)$$

$$P_{CDER}^{min} \cdot U_{y,d,t}^{CDER} \leq P_{y,d,t}^{CDER} \leq P_{CDER}^{max} \cdot U_{y,d,t}^{CDER} \quad (4)$$

$$P_{y,d,t}^{pvcurt} \leq \eta_y^{PV} \cdot P_{y,d,t}^{PV} \cdot S_{PV} \quad (5)$$

$$P_{y,d,t}^{LS} \leq P_{y,d,t}^{load} \quad (6)$$

$$C_{PV}^{deg} = \gamma_{PV}^{rep} \cdot (C_{PV}^{capital} \cdot S_{PV} \cdot \delta_{PV}^{deg}) \quad (7)$$

$$\eta_y^{PV} = \begin{cases} \eta_{init}^{PV}, & y = 1 \\ \eta_{y-1}^{PV} (1 - \delta_{PV}^{deg}), & y > 1 \end{cases} \quad (8)$$

$$SOC_{min} \cdot S_{BESS} \leq E_{y,d,t}^{BESS} \leq SOH \cdot SOC_{max} \cdot S_{BESS} \quad (9)$$

$$SOC_{min} \cdot S_{BESS} \leq E_{y,d,t}^{init} \leq SOH \cdot SOC_{max} \cdot S_{BESS} \quad (10)$$

$$U_{y,d,t}^{chg} + U_{y,d,t}^{dchg} \leq 1 \quad (11)$$

$$P_{y,d,t}^{chg} \leq U_{y,d,t}^{chg} \cdot \frac{S_{BESS}}{T_{BESS}^{chg}} \quad (12)$$

$$P_{y,d,t}^{dchg} \leq U_{y,d,t}^{dchg} \cdot \frac{S_{BESS}}{T_{BESS}^{dchg}} \quad (13)$$

$$E_{y,d,t}^{BESS} = \begin{cases} E_{BESS}^{init} + (\eta_{BESS} \cdot P_{y,d,t}^{chg} - P_{y,d,t}^{dchg}), & y, d, t = 1 \\ E_{y,d,t-1}^{BESS} + (\eta_{BESS} \cdot P_{y,d,t}^{chg} - P_{y,d,t}^{dchg}), & t > 1 \end{cases} \quad (14)$$

$$C_{BESS}^{deg} = \delta_{BESS}^{deg} \cdot \sum_{y \in Y} \sum_{d \in D} \sum_{t \in T} P_{y,d,t}^{dchg} \quad (15)$$

$$\delta_{BESS}^{deg} = \frac{C_{BESS}^{capital} \cdot S_{BESS} \cdot \gamma_{BESS}^{rep}}{S_{BESS} \cdot CL_{dod}} \quad (16)$$

$$P_{y,d,t}^{imp} \leq P_{teline}^{max} \cdot U_{y,d,t}^{imp} \quad (17)$$

$$P_{y,d,t}^{exp} \leq P_{teline}^{max} \cdot U_{y,d,t}^{exp} \quad (18)$$

$$U_{y,d,t}^{imp} + U_{y,d,t}^{exp} \leq 1 \quad (19)$$

The power balance equation (2) ensures the energy supplied by C-DERs, BESS discharging, and PV generation meets the total system demand while accounting for load shedding, PV curtailment, and grid transactions. To maintain operational feasibility, C-DER is subject to lower and upper generation limits, as specified in (3), preventing it from operating outside its allowable capacity range. The constraint governing PV curtailment in (4) quantifies surplus generation, ensuring that any excess solar power beyond immediate demand is either stored, curtailed, or exported, avoiding infeasible overgeneration scenarios. Similarly, load shedding, governed by (5), ensures that any unserved energy is accurately tracked, preventing solution infeasibility.

Long-term system sustainability is reinforced through the inclusion of degradation mechanisms. The degradation cost of PV is formulated in (6), where the financial impact is proportional to system size and follows a constant annual efficiency decline. The degradation of PV efficiency itself is captured in (7), which updates the system's performance over the planning horizon based on an assumed annual degradation factor. The operational limits of BESS are enforced through (8) and (9), where the system's energy level is required to remain within the allowable SOC range, incorporating the effects of SOH degradation over time. Ensuring realistic battery operation, (10) prevents simultaneous charging and discharging, while (11) and (12) constrain the power limits for these processes to mitigate excessive charge rates that accelerate degradation.

Battery energy tracking is implemented through (13), which dynamically updates BESS energy levels by incorporating

efficiency-adjusted charge and discharge cycles. The economic impact of BESS degradation is quantified in (14), where the degradation cost is calculated based on the total discharge energy throughput. The degradation cost factor itself is determined in (15), leveraging a widely adopted linear degradation model that correlates degradation costs with the depth-of-discharge cycle life of the battery [42].

To manage grid interactions, constraints (16) and (17) regulate power imports and exports, ensuring they remain within the allowable tie-line capacity. Simultaneous grid import and export transactions are prevented in (18), ensuring compliance with realistic grid interaction policies. Collectively, these constraints create a comprehensive framework that enforces technical feasibility, accounts for degradation impacts, and ensures economically viable MG operation over the planning horizon.

The formulation in (15) simplifies to (19), effectively eliminating inherent nonlinearities in the degradation model. The nonlinearities in (3), (11), and (12) are eliminated using the BigM method [43]-[44] and the resultant equations are presented below. Thus, the equations defining the integrated multi-year MG planning model are (1), (2), (4)-(10), (13)-(14), and (16)-(27).

$$\delta_{BESS}^{deg} = \frac{C_{BESS}^{capital} \cdot \gamma_{BESS}^{rep}}{CL_{dod}} \quad (19)$$

$$P_{y,d,t}^{CDER} \leq \text{BigM} \cdot U_{y,d,t}^{CDER} \quad (20)$$

$$P_{y,d,t}^{CDER} \leq P_{CDER}^{max} \quad (21)$$

$$P_{y,d,t}^{CDER} \geq \text{BigM} \cdot U_{y,d,t}^{CDER} \quad (22)$$

$$P_{y,d,t}^{CDER} \geq P_{CDER}^{min} \quad (23)$$

$$P_{y,d,t}^{chg} \leq \text{BigM} \cdot U_{y,d,t}^{chg} \quad (24)$$

$$P_{y,d,t}^{chg} \leq \frac{S_{BESS}}{T_{BESS}^{chg}} \quad (25)$$

$$P_{y,d,t}^{dchg} \leq \text{BigM} \cdot U_{y,d,t}^{dchg} \quad (26)$$

$$P_{y,d,t}^{dchg} \leq \frac{S_{BESS}}{T_{BESS}^{dchg}} \quad (27)$$

B. Yearly Validation Model

The yearly validation model extends the benchmark multi-year model by incorporating degradation effects for both PV and BESS, enabling a more accurate assessment of long-term system reliability. While the integrated multi-year model optimizes initial investment decisions without accounting for degradation, the yearly model systematically evaluates the progressive decline in system performance. By updating BESS capacity and efficiency annually based on degradation profiles, this model provides a refined estimation of resource adequacy and operational feasibility over time.

In real-world scenarios, batteries do not operate at a constant DOD unless enforced, leading to varying levels of degradation across different SOC profiles. To accurately model this, the yearly validation model evaluates the SOC profile of the BESS obtained from each yearly simulation, determining the number of cycles at each DOD level and estimating annual degradation. To quantify cyclic degradation, manufacturer-provided cycle life vs. DOD data is required. Figure 3 presents a typical cycle life vs. DOD curve for an LFP battery, illustrating the non-linear relationship between cycle life and DOD [45].

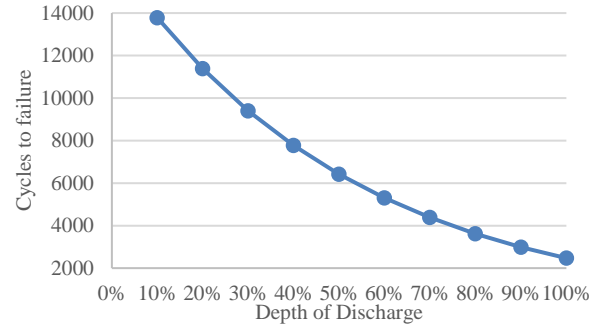


Figure 3. Typical Li-Ion based BESS cycle life vs DOD.

To enhance computational feasibility, a piecewise linearization approach is applied, balancing model accuracy and complexity. The degradation factor for each DOD level, denoted as DF_{dod} is calculated using (28), which quantifies the impact of different DOD levels on cycle life:

$$DF_{dod} = \frac{CL_{dod}^{max}}{CL_{dod}} \quad (28)$$

This factor is used to determine the annual degradation of the BESS capacity, ensuring that the effect of DOD levels is accurately reflected in the degradation model. The net degradation for each year is then calculated using (29)-(32).

$$EFC_y = \alpha \cdot \sum_{dod=1}^n DF_{dod} \cdot CL_y^{dod} \quad (29)$$

$$DPC = \frac{(100\% - EOL\%) \cdot S_{bess}}{\text{cycles at max dod}} \quad (30)$$

$$\text{deg}_y^{BESS} = EFC_y \cdot DPC \quad (31)$$

$$S_{bess_y} = S_{bess_{y-1}} - \text{deg}_y^{BESS}, y > 1 \quad (32)$$

Using the SOC data obtained from the cumulative model, the number of cycles at each distinct DOD level is computed for each year, denoted as CL_y^{dod} and multiplied by the degradation factors for those DOD levels, as shown in (29). The summation of these values provides the equivalent full cycles for the respective year (EFC_y). Using the BESS size from the benchmark model and manufacturer suggested end-of-life (EOL) level, the degradation per cycle (DPC) is then calculated using (30), and the net degradation for the year y (deg_y^{BESS}) is computed using (31). Finally, equation (32) updates the starting BESS size for the following year.

As per existing literature, the efficiency decline in most lithium-based chemistries exhibits a linear trend with respect to SOH. To model this behavior, a linear regression model is applied to efficiency vs. SOH data, allowing for the estimation of updated efficiency values as the BESS degrades.

$$SOH_y = \frac{S_{bess_y}}{S_{bess_{rated}}} * SOH_{init} \quad (33)$$

$$\eta_y^{BESS} = w \cdot SOH_y + b \quad (34)$$

Equation (33) calculates the updated SOH by normalizing the degraded BESS capacity with respect to its initial rated capacity, with 'w' and 'b' denoting the optimal regression coefficients. The computed SOH value acts as an input to (34) which predicts the updated efficiency as a function of SOH.

C. BESS Capacity Iterative Adjustment

The yearly validation model provides critical insights into system reliability and cost-effectiveness by incorporating BESS efficiency and capacity degradation. However, the

results may indicate two key challenges: either positive expected unserved energy (EUE), suggesting the system is insufficient to meet demand, or a suboptimal cost solution due to the exclusion of BESS degradation in the integrated multi-year model. In both cases, increasing BESS size is necessary to ensure zero load shedding. However, it is essential to balance system expansion, as an oversized BESS may eliminate curtailment but significantly increase capital costs. To refine investment decisions while maintaining cost-effectiveness, DBIO employs an iterative optimization process to determine the optimal BESS size, ensuring zero load shedding while minimizing investment costs.

1) Fixed step adjustment

In this method, the BESS size is increased by a fixed increment, and the model is re-solved after each adjustment to evaluate its impact on objective cost and load shedding. The choice of step size plays a crucial role in determining convergence efficiency. A small step size allows for precise identification of the optimal BESS size but requires a large number of iterations, increasing computational burden. Conversely, a larger step size reduces the number of iterations but may overshoot the optimal solution, resulting in a suboptimal cost. While this method is computationally straightforward, it can be time-intensive, especially in high-resolution datasets within the DBIO framework.

2) Binary search-based adjustment

Figure 4 illustrates the binary search refinement process to identify the least-cost solution ensuring zero load shedding. The process begins with initializing a lower bound (LB) at zero, an upper bound (UB) at a large initial value (e.g., double the initial BESS size), and a predefined tolerance for convergence. Load shedding is checked at the current BESS size by re-solving the integrated multi-year and yearly validation optimization problems. If $EUE > 0$, the BESS size is doubled, and the process repeats until no load shedding is detected, updating UB to the current BESS size. Once a feasible range is established, binary search calculates the midpoint between LB and UB, re-solving the optimization problems and checking load shedding. If load shedding occurs, LB is updated to the midpoint; otherwise, UB is updated. This process continues until UB and LB differ by less than the tolerance value, ensuring convergence. The optimal BESS size is set as the midpoint of the final range.

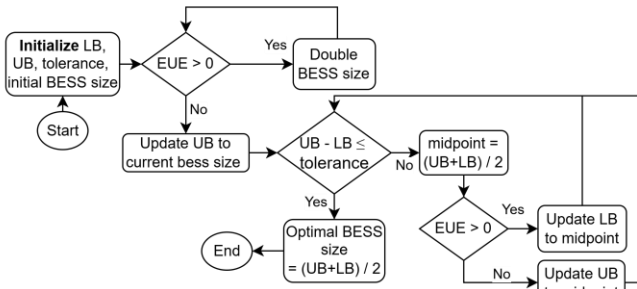


Figure 4. Iterative binary search framework for optimal BESS sizing.

Figure 5 provides an overview of the complete DBIO optimization process, summarizing the key steps from the initial resource investment decision to yearly validation, post-

optimization degradation analysis, parameter updates, and iterative BESS capacity adjustment.

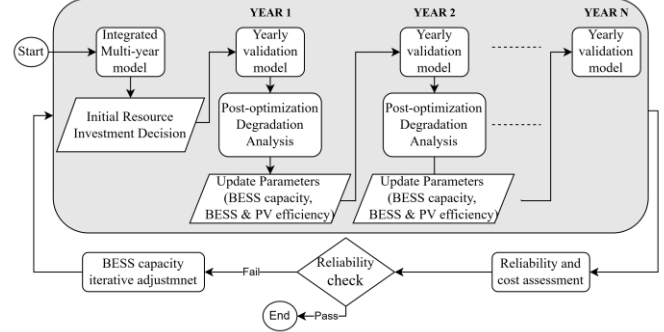


Figure 5. The proposed DBIO framework

The flowchart demonstrates how the methodology ensures reliability and cost-effectiveness by systematically accounting for PV efficiency degradation, BESS capacity fade, and efficiency loss, while refining the system configuration to meet reliability criteria.

IV. CASE STUDIES

The test setup for this study is depicted in Figure 6, representing a grid-connected microgrid supplying a residential area. The grid connection enables both islanded and grid-tied operations, enhancing energy management flexibility and reliability. Three grid tariff structures—Fixed, Time-of-Use (TOU), and Wholesale Market pricing—are considered to analyze economic performance. The fixed tariff is based on Houston’s average residential electricity price [46], TOU rates are taken from a local provider in Houston [47], and wholesale pricing is derived from 2022 Houston Locational Marginal Pricing (LMP) [48]. A net metering scheme is applied where exported electricity is valued 20% lower than the import cost, reflecting industry practices.

The test system consists of a solar PV array, an open-cycle natural gas (NG) turbine as a C-DER, and an LFP-based BESS, chosen for its high energy density, safety, and cycle life. SLBs are also examined to explore cost-saving opportunities. Load data is obtained from the OpenEI TMY2 dataset for Houston, Texas (29.7°N, 95.4°W), with a peak demand of 0.8 MW, a minimum of 0.05 MW, and an average of 0.17 MW per year [49]. The planning horizon spans 25 years, with an assumed 0.5% annual load growth, aligning with typical projections. PV capacity factor data is sourced from NREL’s PVWatts tool [50], configured for Houston’s geographical coordinates to accurately reflect local solar generation potential.

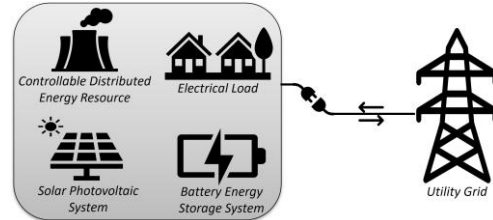


Figure 6. Test system overview.

The selected PV and C-DER characteristics are derived from publicly available sources, emphasizing the practicality of this research [51]-[54]. The PV system has a capital cost of

\$1,450,000 per MW and replacement costs 41% of the initial investment. The NG turbine has a capital cost of \$1,150,000 per MW, with operational and maintenance (O&M) costs of \$44.75 per MWh. The LFP-based BESS has a 90% roundtrip efficiency, 1-hour charge/discharge rate, and \$469,000 per MWh capital cost, with replacement costs at 79% of the initial investment [53], [55]-[56].

This study assumes that the BESS operates within a controlled thermal environment at approximately 25°C. The relationship between DOD and cycle life for a commercially available battery pack highlights the impact of DOD on battery longevity [45]. For instance, batteries discharged at lower DOD levels (10–20%) can sustain between 12,000 and 14,500 cycles, while those discharged at higher DOD levels (90–100%) see reduced cycle life, ranging from 2,000 to 2,200 cycles. These figures are derived using interpolation techniques on manufacturer-provided data, ensuring a realistic representation of battery performance despite the challenges in obtaining detailed experimental data for all DOD levels.

The two MG planning models are implemented on the same test system. The simulation resolution is controlled by the scaling factor ‘ α ,’ which determines how many times the load and solar profiles are repeated within a year. For this study, a full-resolution approach is adopted, using 365 days of hourly data, corresponding to a scaling factor of 1. The solver used is GUROBI 11.0.3, with a MIPGAP setting of 0.0% and a TIME LIMIT setting of 3600 seconds.

The case studies are structured into three key test plans:

- i. Impact of PV Degradation in Islanded Mode – This test evaluates how different PV degradation rates affect system costs, energy utilization, and resource sizing in an MG without grid support.
- ii. Grid Tariffs and SLB Feasibility – This test extends the analysis to a grid-connected MG, comparing different grid tariff structures and the economic viability of SLBs versus new BESS.
- iii. Iterative BESS Sizing for Cost Optimization – This test introduces a binary search-based iterative process to optimize BESS sizing for high-utilization cases, ensuring cost-effectiveness and zero load shedding.

Each test builds on the previous, progressing from fundamental system behavior analysis to investment decision-making and refined optimization. The results provide a comprehensive understanding of how key parameters influence MG planning at different operational conditions.

A. Impact of PV Degradation in Islanded Mode

This section evaluates the impact of PV degradation on the long-term operational and economic performance of an islanded MG. The MG operates independently without grid support, relying solely on a combination of a C-DER, PV panels, and an LFP based BESS. Three test cases are considered to examine how different PV degradation rates influence system costs, energy utilization, and resource sizing.

In Case 1a, no PV degradation is assumed, providing a baseline scenario with idealized PV performance. Case 2a introduces a moderate PV degradation rate of 0.5% per annum, representing realistic but conservative efficiency loss over time. Case 3a models a more aggressive PV degradation scenario of 1% per annum, simulating harsher environmental conditions and aging effects. The economic results of these

three cases are summarized in Table I, which presents a breakdown of capital investment, operational expenses, and degradation costs.

TABLE I. SYSTEM COSTS BREAKDOWN

Attribute	Case 1a	Case 2a	Case 3a
Objective cost (\$)	2,763,400	2,791,429	2,798,968
C-DER capital cost (\$)	957,095	957,651	959,213
PV capital cost (\$)	267,105	222,105	0.0
BESS capital cost (\$)	40,728	40,444	39,648
C-DER operational cost (\$)	1,498,410	1,559,785	1,800,048
PV degradation cost (\$)	0.0	11,383	0.0
BESS degradation cost (\$)	62.75	61.73	59.08

From Table I, it is evident that as PV degradation increases, the optimizer allocates a lower PV capacity to counterbalance efficiency losses. This, in turn, shifts reliance towards the C-DER, leading to a rise in operational costs. Case 3a, with the highest degradation rate, exhibits the most significant increase in C-DER operational expenses due to the diminished PV contribution. The optimal system capacity allocation under varying degradation rates is provided in Table II.

TABLE II. SYSTEM CAPACITY ALLOCATION

Attribute	Case 1a	Case 2a	Case 3a
C-DER size (MW)	0.832	0.833	0.834
PV size (MW)	0.184	0.153	0.000
BESS size (MWh)	0.087	0.086	0.085

As degradation increases, PV sizing trends downward, with Case 3a eliminating PV entirely, shifting reliance to the C-DER and reducing BESS utilization. This suggests that when PV degradation is significant, investing in solar capacity becomes economically unviable for an islanded system. Table III outlines the energy dispatch and utilization trends under different degradation rates.

TABLE III. ENERGY UTILIZATION METRICS

Attribute	Case 1a	Case 2a	Case 3a
Total load (MWh)	40,225	40,225	40,225
C-DER generation (MWh)	33,484	34,856	40,224
PV generation (MWh)	6,872	5,384	0.0
PV curtailed (MWh)	132	10.86	0.0
BESS discharging (MWh)	0.613	0.603	0.577
Load shedding (MWh)	0.000030	0.000028	0.000027

With no PV degradation (Case 1a), PV contributes 17% of the total load, reducing C-DER fuel consumption. However, as degradation increases, PV generation declines, and the C-DER compensates by ramping up production. By Case 3a, PV is fully eliminated, and the C-DER supplies almost the entire load. Interestingly, while the BESS is not explicitly modeled with degradation in this case, minor load shedding is observed due to its limited role in serving demand.

This analysis underscores the significant influence of PV degradation on MG planning. Although its impact may appear minimal in the short term, long-term planning decisions—especially those concerning investment or system expansion—must account for PV efficiency losses to ensure a reliable and cost-effective solution.

B. Grid Tariffs and Second-Life BESS Feasibility

This section examines how grid connectivity, electricity tariff structures, and battery investment strategies influence microgrid planning. Nine distinct cases are analyzed to compare the economic and operational implications of different grid tariffs and battery choices. Three grid pricing structures are considered: Fixed, TOU, and wholesale market

tariff, each affecting energy import/export costs and system operation. Additionally, two battery investment strategies are evaluated—installing a new BESS versus SLBs. SLBs are further classified based on 30% and 70% capital cost reductions, reflecting their lower acquisition costs relative to a new BESS.

Under the fixed tariff scenario (Cases 1b, 2b, and 3b), the microgrid operates with a constant electricity price, optimizing the system for new BESS, SLB (30% cost reduction), and SLB (70% cost reduction), respectively. The TOU tariff scenario (Cases 4b, 5b, and 6b) follows the same battery configurations but applies a variable pricing scheme that encourages strategic energy storage usage during peak demand periods. In the wholesale market tariff scenario (Cases 7b, 8b, and 9b), real-time market fluctuations determine energy costs, directly influencing the microgrid’s energy import/export decisions and BESS utilization.

Since wholesale electricity prices are highly volatile, often fluctuating by thousands of percent above normal values during extreme market conditions, modeling approaches that rely on downscaled temporal resolutions with averaged pricing data fail to capture these uncertainties. Such simplifications may misrepresent real-world conditions, potentially leading to misleading investment decisions and operational strategies. By maintaining a high-resolution approach, this study ensures that dynamic price variations are accurately reflected, providing a more practical and reliable framework for evaluating grid-interactive microgrid performance.

The economic feasibility and optimal resource allocation for each case are summarized in Table IV, presenting the total objective cost, C-DER size, PV capacity, and BESS capacity. The results indicate that grid-tied operation significantly influences the economic viability of the system. Cases utilizing the wholesale tariff (7b-9b) exhibit higher objective costs due to exposure to real-time market volatility, while cases under fixed tariff pricing (1b-3b) benefit from predictable rates, leading to lower costs. Time-of-use tariff cases (4b-6b) show moderate cost variations depending on the alignment of energy production with price fluctuations. The impact of SLBs is particularly evident in cases 3b, 6b, and 9b, where the lowest total objective costs are observed, demonstrating the economic advantage of adopting SLBs despite their lower starting SOH and RTE values.

TABLE IV. OBJECTIVE COST AND SYSTEM SIZING COMPARISON

Case #	Objective cost	C-DER size (MW)	PV size (MW)	BESS size (MWh)
1b	\$1,387,238	0.744	0.000	0.085
2b	\$1,382,431	0.676	0.000	0.338
3b	\$1,168,200	0.462	0.238	2.069
4b	\$1,584,422	0.744	0.000	0.085
5b	\$1,579,509	0.676	0.000	0.338
6b	\$1,361,309	0.456	0.206	2.233
7b	\$2,214,794	0.744	0.000	0.085
8b	\$2,208,620	0.676	0.000	0.338
9b	\$1,994,104	0.444	0.048	2.725

System operation and energy utilization trends further illustrate the impact of grid connectivity and tariff schemes, as presented in Table V. The results indicate that higher BESS capacities facilitate increased PV integration and reduced reliance on C-DER generation. In cases 3b, 6b, and 9b, where SLBs with a 70% cost reduction are adopted, PV capacity is

maximized, and grid imports are minimized, enhancing energy self-sufficiency. Conversely, cases 1b, 4b, and 7b, which rely on new BESS, exhibit greater dependence on C-DERs and limited PV utilization since BESS degradation cost scales with its capital cost.

TABLE V. ENERGY UTILIZATION METRICS (MWH)

Case #	C-DER Gen	PV Gen	BESS Disch	Load shedding	Grid import	Grid Export
1b	59,907	0.0	9.0	0.00047	2.7	19,694
2b	59,866	0.0	32.4	0.00127	5.0	19,678
3b	38,658	7,880	13,261	3.9	45.2	19,583
4b	59,907	0.0	4.1	0.00021	2.7	19,689
5b	59,866	0.0	32.4	0.00127	5.0	19,678
6b	38,781	6,828	14,143	4.0	51.6	19,564
7b	40,919	0.0	0.6	0.00003	7593	8,287
8b	40,907	0.0	5.4	0.00027	7597	8,284
9b	23,607	1,602	16,330	4.7	7284	8,597

Grid interaction also plays a pivotal role in energy dispatch strategies. Cases with wholesale market tariffs (7b-9b) show the highest grid imports, reflecting the impact of real-time price fluctuations, whereas cases under fixed and TOU tariffs (1b-6b) export substantial power, leveraging stable pricing to offset costs. Notably, cases with lower BESS costs exhibit lower degradation costs, leading to greater reliance on BESS for energy storage. As a result, when BESS capacity and efficiency degradation are not accounted for in planning, there is a significant increase in EUE values. While these values remain low in this test system, in scenarios where C-DERs have higher operational costs or strict operational constraints (such as startup, ramping, or no-load costs), EUE values could become considerably high. However, this would not affect the validity of the DBIO modeling approach, as it remains adaptable to diverse planning conditions.

These findings highlight the significant impact of tariff structures and SLBs on MG planning. While wholesale market pricing exposes MG to cost volatility, it allows for flexible dispatch strategies. Fixed and TOU tariffs, in contrast, provide greater cost stability but limit the economic feasibility of large-scale energy storage. The integration of SLBs substantially improves cost-effectiveness by enabling greater energy arbitrage opportunities and reducing capital investment. The results validate that adopting a strategic mix of cost-effective SLBs and optimal tariff selection can significantly enhance the economic viability of grid-connected MGs, supporting their role in future energy systems.

C. Iterative BESS Sizing for Cost Optimization

The final phase of DBIO optimization introduces post-analysis adjustment through an iterative binary search process to refine BESS sizing, ensuring that zero load shedding is achieved with minimal cost. As a BESS operates, its energy capacity degrades and if unaccounted, this degradation may impact system reliability, potentially causing severe energy shortfalls. By dynamically adjusting BESS capacity, DBIO provides a flexible mechanism to mitigate these reliability concerns while optimizing costs.

To illustrate the importance of this approach, we selected Case 9b, the scenario with the highest load shedding, as a test case for iterative refinement. This worst-case scenario highlights the impact of BESS degradation and the need for precise adjustments to maintain system stability. As shown in Figure 7, load shedding increases over time due to BESS

capacity and efficiency fade, when other generation sources and tie-lines reach their limits. Neglecting BESS degradation can severely impact system reliability, emphasizing the need to account for degradation in long-term planning.

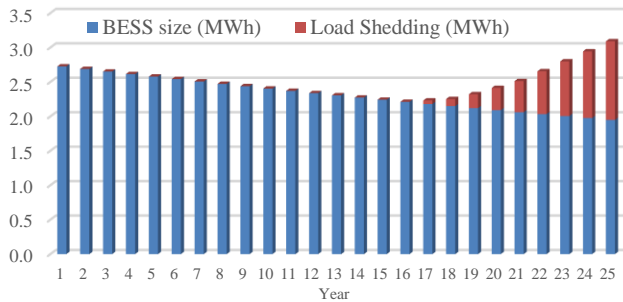


Figure 7. BESS capacity reduction with increasing load shedding for Case 9b.

Figure 8 presents the iteration process for BESS sizing and cost optimization. Iterations marked as ‘YES’ indicate instances where load shedding occurred, while ‘NO’ denotes iterations where the solution met demand without curtailment. Results show that the optimal BESS size ensuring zero load shedding throughout the entire planning horizon including the last year is 3.812 MWh, an increase of 39.9% from the sized capacity of 2.725 MWh obtained with the benchmark model.

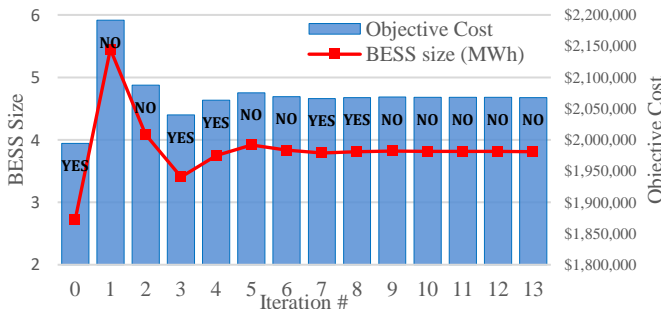


Figure 8. Iterative BESS size and objective cost optimization process.

Through binary search, this result was achieved in just 13 iterations, demonstrating its efficiency in refining investment decisions. By contrast, a fixed step-size approach would have required 40 iterations to reach the same outcome using 1% incremental adjustments, significantly increasing computation time. A step-size of 10% would have resulted in an oversizing at 3.815 MWh, which, while close to the optimal solution in this case, introduces inherent uncertainty in determining the most appropriate percentage increase. This highlights the tradeoff between solution accuracy and convergence speed, reinforcing binary search as the most efficient and adaptive method for optimizing BESS capacity.

The iterative search process in DBIO enables precise determination of the optimal BESS size while maintaining computational efficiency. The results indicate that the binary search-based approach is better suited for this optimization, providing a balanced trade-off between accuracy and computational effort in long-term microgrid planning.

V. CONCLUSION

This study presents a computationally efficient and practical approach for long-term MG planning, addressing PV and BESS degradation while ensuring cost-effectiveness and system reliability. Results highlight that even modest PV efficiency degradation significantly impact investment

decisions, shifting economic preferences towards alternative technologies. Similarly, high-utilization BESS cases reveal that neglecting capacity and efficiency fade risks load shedding, potentially undermining system reliability and increasing costs, particularly in scenarios with high blackout penalties. The proposed DBIO methodology effectively balances these trade-offs, optimizing MG operation over extended planning horizons. By incorporating iterative BESS sizing optimization using binary search, the DBIO framework minimizes load shedding while maintaining cost efficiency. Additionally, sensitivity analysis reveals that SLBs significantly reduce storage costs, enhancing BESS feasibility, while dynamic grid tariffs influence investment strategies. However, SLB adoption depends on achieving sufficient cost reductions to offset performance trade-offs. Future research should focus on quantifying the financial implications of practical and logistical challenges associated with SLB repurposing, ensuring accurate cost-benefit assessments. Overall, the DBIO framework offers a scalable, adaptable solution for microgrid planning, enabling informed investment decisions while accounting for degradation effects, making it valuable for policymakers, utilities, and researchers.

REFERENCES

- [1] A. Bani-Ahmed, A. Nasiri, and H. Hosseini, "Design and development of a true decentralized control architecture for microgrid," *IEEE Energy Conversion Congress and Exposition*, Milwaukee, WI, 2016.
- [2] C. Zhao, J. Silva-Rodriguez, and X. Li, "Resilient operational planning for microgrids against extreme events," *Hawaii Int. Conf. on System Sciences*, Maui, Hawaii, USA, Jan. 2023.
- [3] N. M. Haegel and S. R. Kurtz, "Global progress toward renewable electricity: Tracking the role of solar," *IEEE J. Photovoltaics*, vol. 11, no. 6, pp. 1335-1342, Nov. 2021.
- [4] H. Z. Butt, M. Awon, and H. A. Khalid, "Single phase grid tied PV system modeling and control with low voltage ride-through capability," *Proc. 2019 Int. Conf. on Electrical, Communication, and Computer Engineering (ICECCE)*, Swat, Pakistan, 2019, pp. 1-6.
- [5] J. McDowall, "Energy storage in remote arctic communities: Driving down diesel consumption with batteries," *IEEE Electrification Mag.*, vol. 6, no. 3, pp. 27-33, Sept. 2018.
- [6] R. Fatima, A. A. Mir, A. K. Janjua, and H. A. Khalid, "Testing study of commercially available lithium-ion battery cell for electric vehicle," *Proc. 2018 1st Int. Conf. on Power, Energy and Smart Grid (ICPESG)*, Mirpur Azad Kashmir, Pakistan, 2018, pp. 1-5.
- [7] Q. Ali, H. Z. Butt, and S. A. A. Kazmi, "Integration of electric vehicles as smart loads for demand side management in medium voltage distribution network," *Proc. 2018 Int. Conf. on Computing, Electronic and Electrical Engineering (ICE Cube)*, Quetta, Pakistan, 2018, pp. 1-5.
- [8] M. T. Lawder et al., "Battery energy storage system (BESS) and battery management system (BMS) for grid-scale applications," *Proc. IEEE*, vol. 102, no. 6, pp. 1014-1030, June 2014.
- [9] T. Orhan, G. M. Shafiullah, A. Stojcevski, and A. Oo, "A feasibility study on microgrid for various islands in Australia," *Proc. 2014 Australasian Universities Power Engineering Conf. (AUPEC)*, Perth, WA, Australia, 2014, pp. 1-8.
- [10] M. Huamani Bellido, L. P. Rosa, A. O. Pereira, D. M. Falcão, and S. K. Ribeiro, "Barriers, challenges and opportunities for microgrid implementation: The case of Federal University of Rio de Janeiro," *J. Cleaner Prod.*, vol. 188, pp. 203-216, 2018.
- [11] A. Qamar, A. Patankar, and M. R. Kazmi, "Performance analysis of first grid connected PV power plant in subtropical climate of Pakistan," *Proc. 2018 2nd Int. Conf. on Energy Conservation and Efficiency (ICECE)*, Lahore, Pakistan, 2018, pp. 1-5.
- [12] X. Zheng, Y. Su, L. Wei, J. Zhang, X. Shen, and H. Sun, "Cost-benefit evaluation for battery energy storage considering degradation and data clustering in performance-based frequency regulation service," *Proc. 2020 IEEE 4th Conf. on Energy Internet and Energy System Integration (EI2)*, Wuhan, China, 2020, pp. 279-285.

- [13] X. Zheng, Y. Su, L. Wei, J. Zhang, X. Shen and H. Sun, "Cost-Benefit Evaluation for Battery Energy Storage Considering Degradation and Data Clustering in Performance-Based Frequency Regulation Service," 2020 IEEE 4th Conference on Energy Internet and Energy System Integration (EI2), Wuhan, China, 2020, pp. 279-285.
- [14] "How much do solar panels degrade each year?" Solar Power Genie. [Online]. Available: <https://solarpowergenie.com/how-much-do-solar-panels-degrade-each-year/>
- [15] Statista, "Global battery market size by technology," *Statista*, [Online]. Available: <https://www.statista.com/statistics/1339880/global-battery-market-size-by-technology/>.
- [16] Ziegler and Trancik, "BNEF Long-Term Electric Vehicle Outlook (2023)," *Bloomberg NEF*, 2023.
- [17] McKinsey & Company, "Second-life EV batteries: The newest value pool in energy storage," 2023, [Online]. Available: <https://www.mckinsey.com/industries/automotive-and-assembly/our-insights/second-life-ev-batteries-the-newest-value-pool-in-energy-storage>.
- [18] Cummins, "What happens to lithium-ion batteries at the end of their life," 2021, [Online]. Available: <https://www.cummins.com/news/2021/09/23/what-happens-lithium-ion-batteries-end-their-life>.
- [19] Cabin Radio, "Batteries starting fires at Yellowknife's landfill," 2023, [Online]. Available: <https://cabinradio.ca/102550/news/yellowknife/batteries-starting-fires-at-yellowknifes-landfill-city-says/>.
- [20] WTO, "CATL presentation on circular economy," 2023, [Online]. Available: https://www.wto.org/english/tratop_e/tessd_e/14_circular_economy_5_c_atl_presentation.pdf.
- [21] Battery Stewardship Council, "Why recycle batteries," 2023, [Online]. Available: <https://www.batteryrecycling.org.au/why-recycle>.
- [22] McKinsey & Company, "Second-life EV batteries: The newest value pool in energy storage," 2023, [Online]. Available: <https://www.mckinsey.com/industries/automotive-and-assembly/our-insights/second-life-ev-batteries-the-newest-value-pool-in-energy-storage>.
- [23] A. A. R. Mohamed, R. J. Best, X. Liu, and D. J. Morrow, "Residential battery energy storage sizing and profitability in the presence of PV and EV," in *Proc. IEEE Madrid PowerTech*, 2021, pp. 1–6.
- [24] W. Wei, Z. Wang, F. Liu, M. Shafie-khah, and J. P. S. Catalao, "Cost efficient deployment of storage unit in residential energy systems," *IEEE Trans. Power Syst.*, vol. 36, no. 1, pp. 525–528, Jan. 2021.
- [25] D. Gardiner, O. Schmidt, P. Heptonstall, R. Gross, and I. Staffell, "Quantifying the impact of policy on the investment case for residential electricity storage in the UK," *J. Energy Storage*, vol. 27, Feb. 2020, Art. no. 101140.
- [26] R. Tang, B. Yildiz, P. H. Leong, A. Vassallo, and J. Dore, "Residential battery sizing model using net meter energy data clustering," *Appl. Energy*, vol. 251, 2019, Art. no. 113324.
- [27] M. Gholami, S. A. Mousavi, and S. M. Muyeen, "Enhanced microgrid reliability through optimal battery energy storage system type and sizing," *IEEE Access*, vol. 11, pp. 62733–62743, 2023.
- [28] T. Kerdphol, Y. Qudaih, and Y. Mitani, "Optimum battery energy storage system using PSO considering dynamic demand response for microgrids," *Int. J. Electr. Power Energy Syst.*, vol. 83, pp. 58–66, 2016.
- [29] X. Shen, M. Shahidepour, Y. Han, S. Zhu, and J. Zheng, "Expansion planning of active distribution networks with centralized and distributed energy storage systems," *IEEE Trans. Sustain. Energy*, vol. 8, no. 1, pp. 126–134, Jan. 2017.
- [30] H. Hejazi and H. Mohsenian-Rad, "Energy storage planning in active distribution grids: A chance-constrained optimization with non-parametric probability functions," *IEEE Trans. Smart Grid*, 2017.
- [31] N. Collath, B. Tepe, S. Englberger, A. Jossen, and H. Hesse, "Aging-aware operation of lithium-ion battery energy storage systems: A review," *J. Energy Storage*, vol. 55, p. 105634, 2022.
- [32] Ann Mary Toms, Xingpeng Li, and Kaushik Rajashekara, "Optimal sizing of on-site renewable resources for offshore microgrids," in *Proc. 55th North Amer. Power Symp.*, Asheville, NC, USA, Oct. 2023.
- [33] Y. Zhang, A. Anvari-Moghaddam, S. Peyghami, T. Dragičević, Y. Li, and F. Blaabjerg, "Optimal sizing of behind-the-meter BESS for providing stackable services," in *Proc. 2022 IEEE 13th Int. Symp. Power Electron. Distributed Generation Syst. (PEDG)*, Kiel, Germany, 2022, pp. 1–6.
- [34] W. Diao, S. Saxena, and M. Pecht, "Accelerated cycle life testing and capacity degradation modeling of LiCoO₂-graphite cells," *J. Power Sources*, vol. 435, 2019, Art. no. 226830.
- [35] M. Amini, A. Khorsandi, B. Vahidi, S. H. Hosseini, and A. Malakmahmoudi, "Optimal sizing of battery energy storage in a microgrid considering capacity degradation and replacement year," *Electr. Power Syst. Res.*, vol. 195, p. 107170, 2021.
- [36] A. A. R. Mohamed, R. J. Best, X. Liu, and D. J. Morrow, "A comprehensive robust techno-economic analysis and sizing tool for the small-scale PV and BESS," *IEEE Trans. Energy Convers.*, vol. 37, no. 1, pp. 560–572, Mar. 2022.
- [37] S. Paul, A. P. Nath, and Z. H. Rather, "A multi-objective planning framework for coordinated generation from offshore wind farm and battery energy storage system," *IEEE Trans. Sustain. Energy*, vol. 11, no. 4, pp. 2087–2097, Oct. 2020.
- [38] L. Ahmadi, M. Fowler, S. B. Young, R. A. Fraser, B. Gaffney, and S. B. Walker, "Energy efficiency of Li-ion battery packs re-used in stationary power applications," *Sustainable Energy Technologies and Assessments*, vol. 8, pp. 9-17, 2014.
- [39] Y. Tao, C. D. Rahn, L. A. Archer, and F. You, "Second life and recycling: Energy and environmental sustainability perspectives for high-performance lithium-ion batteries," *Science Advances*, vol. 7, no. 45, article eabi7633, 2021, doi:10.1126/sciadv.abi7633.
- [40] M. Elliott, L. G. Swan, M. Dubarry, and G. Baure, "Degradation of electric vehicle lithium-ion batteries in electricity grid services," *Journal of Energy Storage*, vol. 32, p. 101873, 2020.
- [41] C. Beckers, E. Hoedemaekers, A. Dagkicil and H. J. Bergveld, "Round-Trip Energy Efficiency and Energy-Efficiency Fade Estimation for Battery Passport," 2023 *IEEE Vehicle Power and Propulsion Conference (VPPC)*, Milan, Italy, 2023, pp. 1-6.
- [42] C. Zhao, X. Li, and Y. Yao, "Quality analysis of battery degradation models with real battery aging experiment data," *IEEE Texas Power Energy Conf. (TPEC)*, College Station, TX, USA, 2023.
- [43] R. Fatima, H. Z. Butt, and X. Li, "Optimal dynamic reconfiguration of distribution networks," *North Amer. Power Symp. (NAPS)*, Asheville, NC, USA, 2023, pp. 1–6.
- [44] Q. Wang and X. Li, "Evaluation of battery energy storage system to provide virtual transmission service," *Electric Power Systems Research*, Feb. 2025.
- [45] BSLBATT, "Lithium Iron Phosphate (LFP or LiFePO₄)," 2019. [Online]. Available: <https://www.lithium-battery-factory.com/lithium-iron-phosphate-lifepo4/>
- [46] U.S. Energy Information Administration, "Average retail price of electricity," *Electric Power Monthly*, [Online]. Available: https://www.eia.gov/electricity/monthly/epm_table_grapher.php?t=epmt_5_6_a&form=MG0AV3.
- [47] Rhythm Energy, "Shift – Smart Energy Plan," [Online]. Available at: <https://www.gotrhythm.com/shift>.
- [48] U.S. Energy Information Administration, "ERCOT LMP data for 2022," [Online]. Available at: <https://www.eia.gov/electricity/wholesalemarkets/data.php?rto=ercot>.
- [49] S. Ong and N. Clark, Commercial and Residential Hourly Load Profiles for all TMY3 Locations in the United States, U.S., 25 Nov. 2014.
- [50] National Renewable Energy Laboratory (NREL), "PVWatts calculator." [Online]. Available: <https://pvwatts.nrel.gov/index.php>
- [51] Lazard, Lazard's Levelized Cost of Energy Analysis—Version 15.0, 2021. [Online]. Available: <https://www.lazard.com/media/sptlfats/lazards-levelized-cost-of-energy-version-150-vf.pdf>
- [52] M. Tobias, "Breaking down the price of solar power systems," NY Engineers. [Online]. Available: <https://www.ny-engineers.com/blog/breaking-down-the-price-of-solar-power-systems>
- [53] Lazard, 2023 Levelized Cost of Energy+, 2023. [Online]. Available: <https://www.lazard.com/research-insights/2023-levelized-cost-of-energyplus/>
- [54] Approximate Natural Gas Consumption Chart. Generator Source. [Online]. Available: https://www.generatorsource.com/Natural_Gas_Fuel_Consumption.aspx
- [55] M. Safoutin, J. Cherry, J. McDonald, and S. Lee, "Effect of current and SOC on round-trip energy efficiency of a lithium-iron phosphate (LiFePO₄) battery pack," *SAE Tech. Paper 2015-01-1186*, 2015.
- [56] T. Steckel, A. Kendall, and H. Ambrose, "Applying levelized cost of storage methodology to utility-scale second-life lithium-ion battery energy storage systems," *Appl. Energy*, vol. 300, 2021, Art. no. 117309.